Journal of Theoretical Biology 520 (2021) 110658

Contents lists available at ScienceDirect

Journal of Theoretical Biology

journal homepage: www.elsevier.com/locate/yjtbi

Modelling cell guidance and curvature control in evolving biological tissues

Solene G.D. Hegarty-Cremer [a], Matthew J. Simpson [a], Thomas L. Andersen [b,c,d], Pascal R. Buenzli [a,*]

[a] School of Mathematical Sciences, Queensland University of Technology (QUT), Brisbane, Australia
[b] Clinical Cell Biology, Department of Pathology, Odense University Hospital, Odense, Denmark
[c] Pathology Research Unit, Department of Clinical Research, University of Southern Denmark, Odense, Denmark
[d] Department of Forensic Medicine, Aarhus University, Aarhus, Denmark

ARTICLE INFO

Article history:
Received 15 July 2020
Revised 20 January 2021
Accepted 26 February 2021
Available online 02 March 2021

Keywords:
Tissue growth
Bone remodelling
Tissue engineering
Surfactant
Moving boundary problems

ABSTRACT

Tissue geometry is an important influence on the evolution of many biological tissues. The local curvature of an evolving tissue induces tissue crowding or spreading, which leads to differential tissue growth rates, and to changes in cellular tension, which can influence cell behaviour. Here, we investigate how directed cell motion interacts with curvature control in evolving biological tissues. Directed cell motion is involved in the generation of angled tissue growth and anisotropic tissue material properties, such as tissue fibre orientation. We develop a new cell-based mathematical model of tissue growth that includes both curvature control and cell guidance mechanisms to investigate their interplay. The model is based on conservation principles applied to the density of tissue synthesising cells at or near the tissue's moving boundary. The resulting mathematical model is a partial differential equation for cell density on a moving boundary, which is solved numerically using a hybrid front-tracking method called the cell-based particle method. The inclusion of directed cell motion allows us to model new types of biological growth, where tangential cell motion is important for the evolution of the interface, or for the generation of anisotropic tissue properties. We illustrate such situations by applying the model to simulate both the resorption and infilling components of the bone remodelling process, and to simulate root hair growth. We also provide user-friendly MATLAB code to implement the algorithms.

1. Introduction

Understanding the mechanisms controlling the generation of biological tissue is an important challenge in biomechanics and mechanobiology (Ambrosi et al., 2019) with key applications in tissue engineering and developmental biology (O'Brien, 2011; Dzobo et al., 2018). Tissue geometry influences the generation of new tissue, particularly the rate of tissue growth and the organisation of tissue material (Curtis and Varde, 1964; Dunn and Heath, 1976; Kollmannsberger et al., 2011). Several tissue growth experiments show that the rate of tissue progression is strongly dependent on tissue curvature. These findings apply to bioscaffold pore infilling (Bidan et al., 2015; Bidan et al., 2016; Guyot et al., 2014; Ripamonti and Roden, 2010), wound healing (Poujade M., 2007; Rolli et al., 2012), tumour growth (Lowengrub et al., 2010), and bone remodelling (Martin, 2000; Alias, 2018). This proportionality of growth rate and curvature may be caused by the crowding and spreading of cells and tissue material due to spatial constraints, and curvature-dependent tissue surface tension influencing cell proliferation rates (Nelson et al., 2005; Rumpler et al., 2008; Haeger et al., 2015; Alias, 2017; Buenzli et al., 2020).

In addition to the collective influence of curvature on tissue progression, other factors such as mechanical or chemical cues in the environment as well as cell-scale geometrical features can induce individual cell responses including directed cell migration. Mechanical cues include viscoelasticity (Chaudhuri et al., 2016), surface stiffness (Pelham and Wang, 1997; Lo et al., 2000; Discher et al., 2005; Engler et al., 2006), or surface mechanical stretch (Trepat et al., 2007; Bouchbinder et al., 2014). Chemical cues include signalling molecules inducing attractive or repulsive chemical gradients (Haeger et al., 2015), and cell-scale geometrical cues include geometrical guidance such as curvotaxis (Callens et al., 2020) and surface roughness gradients (Martin et al., 1995; Deligianni and Katsala N.D., 2001). While the collective influence of curvature on tissue growth and the effects of environmental cues on cell guidance mechanisms are well studied in isolation, how these processes interact during the generation of new biological tissue remains poorly understood.

* Corresponding author.
E-mail address: pascal.buenzli@qut.edu.au (P.R. Buenzli).

https://doi.org/10.1016/j.jtbi.2021.110658
0022-5193/

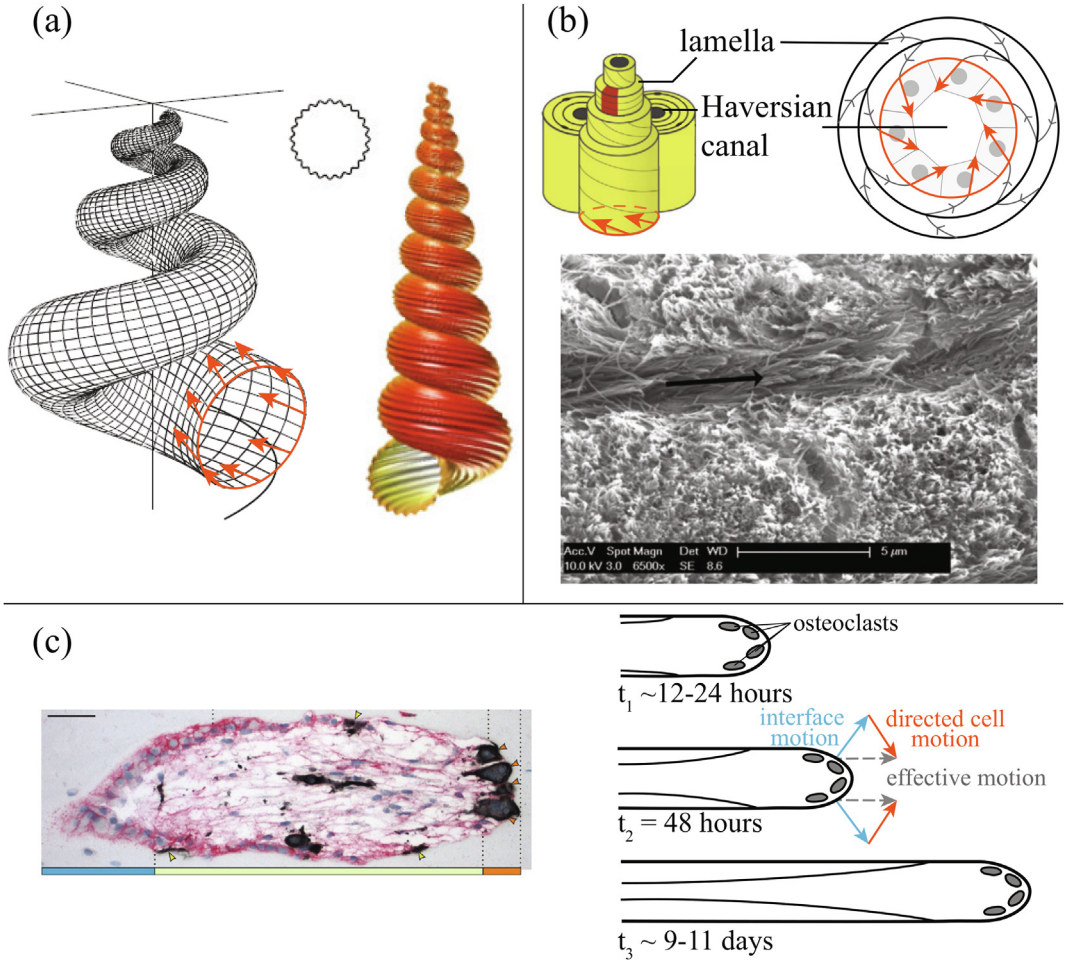

Fig. 1. Tangential cell movement in tissue growth. (a) Shells grow by secretion of new tissue at their base (mantle) at an angle to create spiralling structures (reproduced with permissions from Goriely (2017)). (b) In lamellar bone, successive tissue layers possess different collagen fibril orientations which suggest changes in the tangential motion of osteoblasts during bone formation (reproduced with permissions from Pazzaglia et al. (2012) and Schrof et al., 2014). (c) Resorption cavities during bone resorption maintain a stable resorption front shape at the tip. Since the dissolution process of bone by osteoclasts is expected to occur in the normal direction, this suggests osteoclasts are subject to cell guidance signals toward the cavity centerline. An example of the serial section of a cutting cone, immunostained (black) for an osteoclastic marker, obtained from Lassen et al. (2017) and schematic of an evolving Haversian system, after Jaworski and Hooper (1980).

In this work we develop a new mathematical model which explicitly includes both the collective influence of curvature and directed cell guidance mechanisms. The addition of directed cell guidance allows us to model new types of biological growth, which cannot be generated by existing mathematical models where the tissue interface progresses in the normal direction only (Bidan et al., 2015; Guyot et al., 2014; Alias, 2017; Callens et al., 2020).

Indeed, the growth of several tissues involves directed cell motion where cells move tangentially along the tissue surface (Fig. 1). For example, shells, horns, and tusks with a spiralling structure are generated by tissue being secreted at an angle to the base membrane (Fig. 1a) (Skalak et al., 1982; Skalak et al., 1997). Tangential cell velocity may also be responsible for the generation of anisotropies in tissue material properties by aligning tissue fibrils with respect to the cells motion (Fig. 2). In lamellar bone, the so-called twisted plywood structure of collagen fibrils may be due to the osteoblasts (bone secreting cells) changing direction of motion during bone infilling (Martin et al., 2004) (Fig. 1c). Finally, tangential cell motion is suspected to occur in bone resorption to keep osteoclasts at the front of the resorption cone (Fig. 1c).

Mathematically, the evolution of *smooth* interfaces can be described by the normal velocity of the interface only (Sethian, 1999). However, biological tissue interfaces may develop cusps

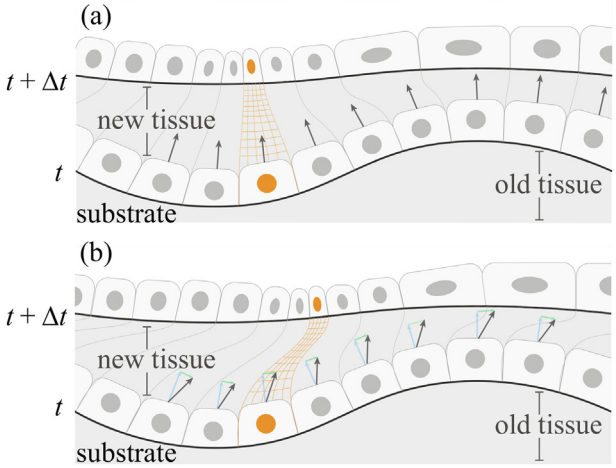

Fig. 2. Schematic illustrating the crowding and spreading effect of curvature and the influence of tangential motion for tissue material properties; (a) shows only movement in the normal direction and the resulting changes in density; (b) includes both curvature control and cell guidance, meaning the cells crowd and spread and also undergo directed motion, creating anisotropies in tissue material properties (thin orange lines).

and sharp edges (Skalak et al., 1997; Alias, 2017; Goriely, 2017). When these move at an angle to their base, one is required to consider a more general tissue interface velocity that includes a tangential component to avoid the emergence of singularities in the governing equation for tissue growth velocity (Skalak et al., 1997).

Many existing models of geometric control of tissue growth consider the geometry of the tissue substrate only, so that cell guidance mechanisms and cell crowding effects are not modelled explicitly (Skalak et al., 1982; Skalak et al., 1997; Rumpler et al., 2008; Bidan et al., 2012; Bidan et al., 2015; Gamsjäger et al., 2013; Guyot et al., 2014; Goriely, 2017; Ehrig et al., 2019). Here, we consider the cell-based mathematical model of Alias (2017), which explicitly accounts for curvature-induced cell crowding and spreading, and we generalise this model to allow for tangential cell motion. We derive the model from general conservation properties imposed on cells, which allows us to explicitly include cell behaviours. To our knowledge, no mathematical model currently includes both the effect of curvature on collective cell crowding and spreading and tangential cell motion mechanisms.

The model of Alias (2017) is also extended to three dimensions and the governing equations are derived in covariant form. The model derived is a partial differential equation (PDE) for the density of cells to be solved on a moving boundary, which represents the evolving tissue surface. This problem is numerically solved to explore several situations in which tangential cell guidance mechanisms are added. We demonstrate that with the addition of tangential cell advection, new biologically relevant tissue growth phenomena can be modelled, such as bone resorption, the generation of different fibre orientations in lamellar bone, and root hair growth.

2. Description of the model

Tissue growth usually occurs by cells synthesising new tissue close to the tissue's interface. To determine general evolution equations for the density of tissue-synthesising cells subject to normal and tangential motion, we consider the case where the tissue-synthesising cells are attached to the tissue interface and described by a surface density, ρ (number of cells per unit surface). The motion of the interface transports the cells in space and the cells may additionally move laterally with respect to the material points of the surface. The motion of the interface is considered to be due to new tissue being synthesised in the wake of these surface-bound cells (Fig. 2). This situation occurs for example in wound healing, bone remodelling, bioscaffold pore infilling, and tumour growth (Guyot et al., 2014; Bidan et al., 2015; Lowengrub et al., 2010; Poujade M., 2007; Rumpler et al., 2008) where tissue-synthesing cells are located at or near the tissue interface. The normal velocity of the tissue interface, $u_n\mathbf{n}$ where $\mathbf{n}$ is the outward-facing unit surface normal, is given by

$$u_n = k\rho, \tag{1}$$

where k is the tissue-synthesising cells' secretory rate (volume of new tissue synthesised per unit time per cell) (Buenzli, 2015). Tissue resorption can also be modelled by assuming k to be negative. Although in this derivation we take ρ to denote the density of tissue-secreting cells, other situations can be modelled if ρ is taken as the density of other surface-bound tissue-secreting entities, such as secretory vesicles (see Section 3.4).

During the evolution of the tissue, the interface may stretch locally depending on its curvature (Fig. 2a), and this will induce changes in cell density. Convex areas of the tissue substrate result in cells spreading whereas concave areas of the tissue substrate result in cells crowding. In addition, cell guidance mechanisms superimpose lateral cell motion with respect to the tissue interface. Directional tissue growth may therefore result from a combination of interface motion and lateral cell motion (Figs. 2b and 3).

The tangential velocities of both the interface and the cells can be chosen to describe multiple biological tissue evolution scenarios. The tangential velocity of the cells, $\mathbf{v}_S$, can represent for example epithelial cells moving with respect to a basal membrane which may itself be transported in space with velocity $\mathbf{u}$. Biological situations where cells are not physically transported by a moving tissue interface may be modelled by assuming that there is no tangential movement of the interface ($\mathbf{u}_S = 0$, where $\mathbf{u}_S$ is the tangential component of $\mathbf{u}$) while cells may still have tangential velocity ($\mathbf{v}_S \neq 0$). This can occur in the case of bone resorption for example, where material points of the bone interface do not move laterally but osteoclasts living on the interface may (Lassen et al., 2017). It is important to note that although the velocity of the tissue surface and the cells may not be distinguishable for modelling the evolution of the tissue interface and changes in cell density, the distinction between these velocities can be important for modelling the tissue material properties produced (Fig. 2b, Buenzli (2016)), as we will illustrate in our application of the model to bone formation (see Section 3.2).

The tissue interface is denoted by $S(t)$ and $\rho(\mathbf{r}_S, t)$ denotes the surface density of the tissue-synthesising cells, at position $\mathbf{r}_S$ on $S(t)$. We formally define $\rho(\mathbf{r}_s, t)$ by considering an infinitesimal element of surface δS at position $\mathbf{r}_s$ of $S(t)$, and the number of cells living on this area, δN. It is important to choose δS small enough to capture heterogeneous densities but large enough to contain a suf-

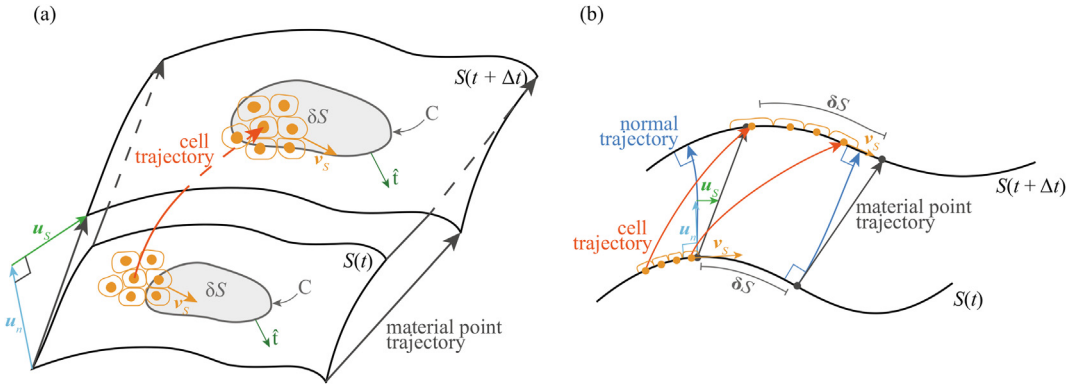

Fig. 3. (a) Schematic of two dimensional surface portion being considered. The curve C surrounding δS is illustrated as well as its outward facing normal $\hat{\mathbf{t}}$. (b) One dimensional schematic of portion of interface being examined. The normal and tangential components of the surface velocity are annotated in blue and green respectively. Illustrative cells are included in orange, with the tangential flux of cells into $\delta\mathbf{S}$ annotated in orange. The grey arrows indicate the material trajectories of the surface. Cell trajectories and normal trajectories are also annotated.

ficient number of cells to define a continuous surface density of cells, such that

$$\rho = \frac{\delta N}{\delta S}. \tag{2}$$

We now derive a conservation law for the surface density of cells living on the evolving surface as the tissue evolves. To do so, we consider the material derivative of ρ following the material trajectories, $\mathbf{r}_S(t)$, of the surface $S(t)$, defined as

$$\left(\frac{\partial \rho}{\partial t}\right)_{\mathbf{m}} = \frac{\mathrm{d}}{\mathrm{d}t}\,\rho(\mathbf{r}_S(t), t).$$

The material derivative obeys standard rules of differentiation, so that differentiating Eq. (2) gives

$$\left(\frac{\partial \rho}{\partial t}\right)_{\mathbf{m}} = \frac{1}{\delta S}\left(\frac{\partial \delta N}{\partial t}\right)_{\mathbf{m}} - \frac{\rho}{\delta S}\left(\frac{\partial \delta S}{\partial t}\right)_{\mathbf{m}}. \tag{3}$$

The first term on the right hand side of Eq. (3) corresponds to changes in density induced by changes in the number of cells residing in δS. The second term on the right hand side of Eq. (3) describes changes in cell density due to local changes in the area of the portion of interface δS during its evolution. In the first term, the number of cells may change due to proliferation, death, or net transport from the surrounding portions of the surface. The change in cell number due to proliferation and elimination can be expressed by $(P - A)\delta N(t)$ where P is the per capita proliferation rate, and A is the per capita cell elimination rate. The cell elimination rate may model cell death (apoptosis), detachment from the surface (for example anoikis), or embedment into the tissue. To describe the influence of tangential motion of the cells on cell density changes at position $\mathbf{r}_s$, we introduce the tangential flux of cells, $\mathbf{J}(\mathbf{r}_S, t)$. This cell flux is measured with respect to material points of the surface, which are themselves transported in space. It represents the number of cells crossing the boundary C of δS per unit length per unit time (Fig. 3a). The total number of cells leaving and entering δS is thus calculated by the line integral of the flux of cells along C, where C is the curve surrounding δS, with unit normal given by $\hat{\mathbf{t}}$ (Fig. 3a). Therefore, the total rate of change of cell number in δS is

$$\left(\frac{\partial \delta N}{\partial t}\right)_{\mathbf{m}} = -\oint_C \mathbf{J}\cdot\hat{\mathbf{t}}\,\mathrm{d}l + (P - A)\delta N(t). \tag{4}$$

Since δS is a small element of surface, the line integral in Eq. (4) can be written in terms of the surface divergence of $\mathbf{J}$, which can be formally defined as

$$\nabla_S \cdot \mathbf{J} = \frac{1}{\delta S}\oint_C \mathbf{J}\cdot\hat{\mathbf{t}}\,\mathrm{d}l, \qquad \text{as} \quad \delta S \to 0 \tag{5}$$

(Arnoldus, 2006). Thus, in the limit of an infinitesimally small area of the interface δS, the change in density due to the change in number of cells in δS in Eq. (3) is given by

$$\frac{1}{\delta S}\left(\frac{\partial \delta N}{\partial t}\right)_{\mathbf{m}} = -\nabla_S \cdot \mathbf{J} + (P - A)\rho. \tag{6}$$

Eq. (6) represents the fact that the surface divergence of the flux on a curved manifold is related to local changes in surface density (Arnoldus, 2006), much like, in the Euclidean space, the divergence of the flux is related to local changes in volumetric density.

To evaluate the second term of on the right hand side of Eq. (3), we examine the rate at which δS changes following the material trajectories of $S(t)$. This depends on the local mean curvature,

$$\kappa = \nabla_S \cdot \mathbf{n}, \tag{7}$$

and is given by

$$\left(\frac{\partial(\delta S)}{\partial t}\right)_{\mathbf{m}} = \delta S(u_n\kappa + \nabla_S \cdot \mathbf{u}_S). \tag{8}$$

where $\mathbf{u}_S$ is the tangential component of the surface velocity and $\mathbf{u}$ (Fig. 3). Eq. (8) is derived using the equation for the change of a material area element over time from Batchelor (1967), see A for details. In our notation, κ is defined such that $\kappa < 0$ indicates concavity and $\kappa > 0$ indicates convexity.

Substituting Eqs. (6) and (8) into Eq. (3), we find that the evolution of the surface density of cells following material trajectories of the interface is governed by

$$\left(\frac{\partial \rho}{\partial t}\right)_{\mathbf{m}} = -\nabla_S \cdot \mathbf{J} - \rho u_n\kappa - \rho\nabla_S \cdot \mathbf{u}_S + (P - A)\rho. \tag{9}$$

If cell migration includes advection and diffusion, the tangential flux of cells can be written as

$$\mathbf{J} = \rho\mathbf{v}_S - D\nabla_S\,\rho, \tag{10}$$

where $\mathbf{v}_S$ is the tangential velocity of the cells with respect to the surface and $-D\nabla_S\,\rho$ corresponds to lateral diffusive flux along the curved interface where ∇_S is the surface gradient of ρ, that is the derivative of ρ on the manifold $S(t)$ (Pressley, 2010). In this case, the evolution of the surface density of cells, Eq. (9) becomes

$$\left(\frac{\partial \rho}{\partial t}\right)_{\mathbf{m}} = D\nabla_S^2\rho - \nabla_S \cdot (\rho\mathbf{v}_S) - \rho\nabla_S \cdot \mathbf{u}_S - \rho u_n\kappa + (P - A)\rho. \tag{11}$$

It is possible to determine the rate of change of cell density following other trajectories than the material points of the interface. The evolution equation for cell density takes a particularly convenient form when expressed following trajectories normal to the interface at each time (Fig. 3). We can relate the derivatives of ρ along the normal and material trajectories by

$$\left(\frac{\partial \rho}{\partial t}\right)_{\mathbf{n}} = \left(\frac{\partial \rho}{\partial t}\right)_{\mathbf{m}} - \mathbf{u}_s \cdot \nabla_S\rho \tag{12}$$

where $(\partial/\partial t)_{\mathbf{n}}$ represents the time derivative along the normal trajectories, that is trajectories perpendicular to the surface at all times (Wong et al., 1996). Substituting Eq. (11) into Eq. (12) gives

$$\left(\frac{\partial \rho}{\partial t}\right)_{\mathbf{n}} = D\nabla_S^2\rho - \nabla_S \cdot (\rho(\mathbf{v}_S + \mathbf{u}_S)) - \rho u_n\kappa + (P - A)\rho. \tag{13}$$

The first term on the right hand side of Eq. (13) is the Laplace–Beltrami operator applied to the surface density of cells and describes the tangential diffusion of cells along the curved tissue surface (Berger, 2003). The second term describes the influence of tangential velocities of the cells $\mathbf{v}_S$ and of the tissue surface $\mathbf{u}_S$, respectively. The fourth term encapsulates the collective cell crowding or spreading effect of curvature, and the last term describes the gain or loss of cells from the group of tissue-synthesising cells. Eqs. (11) and (13) are general conservation equations for cells moving by advection and diffusion with respect to a surface which is itself moving and deforming. In B, we show that these equations are a generalisation of similar conservation equations of surface-bound quantities derived in the literature without tangential advection.

In our applications, for simplicity in the numerical solution, we will look at two dimensional problems where the interface is described by a one-dimensional tissue interface, that is, a curve in two-dimensional space. In these situations, Eq. (13), can be written as

$$\left(\frac{\partial \rho}{\partial t}\right)_{\mathbf{n}} = D\frac{\partial^2}{\partial l^2}\rho - \rho u_n\kappa - \frac{\partial}{\partial l}(\rho(v_S + u_S)). \tag{14}$$

where $\partial/\partial l$ is the derivative with respect to the arc length of the surface, which is the one dimensional equivalent of the surface divergence and surface gradient (Redžić, 2001). In the applications presented in Section 3, we solve the coupled Eqs. (1) and (14),

where the tangential cell velocity is given various forms and the ensuing behaviour is analysed.

2.1. Numerical method

Solving Eqs. (1) and (14) requires solving a PDE on a moving boundary where the boundary motion is coupled with the PDE solution. To achieve this, we use an efficient hybrid computational method, the cell-based particle method (CBPM), developed in Leung and Zhao (2009), Leung et al. (2011) and Hon et al. (2014). In this method, the interface is represented by Lagrangian marker particles which are each associated with a grid cell of an underlying Eulerian grid with grid cell length Δx. The grid is used to redistribute the particles along the moving interface to maintain quasi-uniform sampling. Furthermore, scalar quantities, such as cell density, can be associated directly with the marker particles (Leung and Zhao, 2009). This is an advantage over level-set like methods, which require additional scalar fields similar to the level-set function to represent surface-bound quantities (Alias and Buenzli, 2019). The interface is evolved over discretised timesteps Δt by advecting the marker particles according to a velocity field. Local quadratic least squares interpolation of the interface and of the surface density of cells is then used to estimate the interface curvature and to evaluate spatial derivatives. The reader is referred to the Supplementary Information, Leung and Zhao (2009), Leung et al. (2011), Hon et al. (2014) and Hegarty-Cremer (2020) for more details.

3. Results

We now apply our mathematical model to cases of tissue growth where the inclusion of tangential cell advection allows us to model new biologically relevant situations. First, we validate the numerical method by solving simplified equations which test the two migration mechanisms of Eq. (14), that is tangential cell advection and diffusion, as well as the crowding and spreading effect of curvature. These solutions are compared with analytic solutions. Then we model bone pore infilling and explore the generation of different orientations of collagen fibrils in infilled osteons, as illustrated in Fig. 1b. We also model bone resorption, where osteoclasts tunnel through old bone tissue and investigate the influence of tangential cell velocity for the stability of travelling-wave-like resorption fronts observed during the resorption of cortical bone. Finally, we model the apical growth of root hairs and compare cell membrane trajectories and membrane curvature maps to experimental data (Shaw et al., 2000; Goriely, 2017).

3.1. Validation of the numerical method

To validate our implementation of the CBPM for solving Eq. (14), we compare numerical simulations to analytical solutions in a simple setting where the governing equations are non-dimensionalised. To simplify the problem, the density is decoupled from the normal speed of the interface, that is we replace Eq. (1) with $u_n = c$, where c is a constant. We also set $D = 0$ and choose a circular initial interface with initial radius R_0. In this case, the interface remains a circle at all times and it expands in the normal direction with radius $R(t)$. We parameterise the circle using the arc length l and solve for ρ on the domain $-\pi < l < \pi$. The governing equations become

$$\frac{\mathrm{d}R}{\mathrm{d}t} = c \tag{15}$$

$$\frac{\partial \rho}{\partial t} + v_S \frac{\partial \rho}{\partial l} = \frac{\partial v_S}{\partial l}\rho - \rho c \kappa. \tag{16}$$

We assume an arbitrary initial cell density distribution $\rho(l,0) = \rho_0(l)$ and an initial radius $R(0) = R_0$, and impose periodic boundary conditions $\rho(-\pi, t) = \rho(\pi, t)$. The solution for $R(t)$ is

$$R(t) = ct + R_0, \tag{17}$$

so that $\kappa(t) = 1/(ct + R_0)$. To test the advection term in Eq. (14), we assume that cells are subject to the tangential cell velocity field $v_S = -al$ where a is constant. The governing equation for ρ becomes a quasilinear advection equation, which can be solved using the method of characteristics (Evans, 2010), giving

$$\rho(l,t) = \frac{\rho_0(le^{at})R_0 e^{at}}{ct + R_0}. \tag{18}$$

We test numerically both dilution of cells without advection, $a = 0$, and dilution of cells with advection, $a \neq 0$. Fig. 4 compares this analytical solution to the numerical solution obtained using the CBPM. In Fig. 4, the initial condition for density is piecewise constant such that $\rho = 0.5$ when $\pi/8 < |l| < 3\pi/8$ and $\rho = 0$ elsewhere. There is excellent alignment between the analytic solution in Eq. (18) and the one obtained by the CBPM both with and without tangential velocity. The small discrepancies are due to some degree of smoothing of the numerical solution, which originates from the local interpolation step of the CBPM. As expected, if the numerical discretisation is refined, the match improves. Convergence graphs can be found in the Supplementary Information, Figure S1.

To validate our implementation of the CBPM for problems that include diffusive transport, we solve the diffusion equation on a stationary circle using the CBPM. With a sinusoidal initial condition $\rho_0(l) = 0.5 + 0.5\sin(l)$ and periodic boundary conditions the analytic solution is given by

$$\rho(l,t) = 0.5 + 0.5\sin(l)e^{-4Dt}. \tag{19}$$

The results of the CBPM are compared with this solution at different times in Fig. 5. Again, there is an excellent agreement between the solutions.

3.2. Circular bone pore infilling

We now consider the case of a circular bone pore being infilled by a population of osteoblasts distributed uniformly along the pore's perimeter. This can be thought of as the infilling of a cortical bone osteon seen in a transverse cross section. New bone tissue is gradually produced such that the initial interface is moving inwards while retaining a circular shape. As infilling proceeds, the density increases as a result of the systematic effect of curvature (Buenzli et al., 2014; Buenzli, 2016). We examine three cases of tangential cell velocity: no tangential velocity, constant tangential cell velocity, and time-dependent tangential cell velocity such that cells reverse their motion with respect to the interface at specific times (Fig. 6). By rotation symmetry, in these simulations, the density remains uniform at all times, but it is time dependent due to the shrinkage of the bone surface area as infilling proceeds. The model parameters in Fig. 6 are based on experimental values, see Alias (2018) for more details.

The evolution of density and interface position is the same across the three cases (Figs. 6a–c). However, the cell trajectories in space are distinct, and this creates different tissue material properties (Figs. 6d–f). To visualise cell trajectories in Figs. 6, d–f, cells are stained either in blue or in yellow. This is achieved in the CBPM by assigning a new scalar property to each marker particle, which is simply advected along the cell trajectories. In Fig. 6d, cells have no tangential motion hence their trajectories are moving along straight radial lines. However, in Figs. 6e and 6f, the cells move tangentially to the surface, thus their trajectories spiral

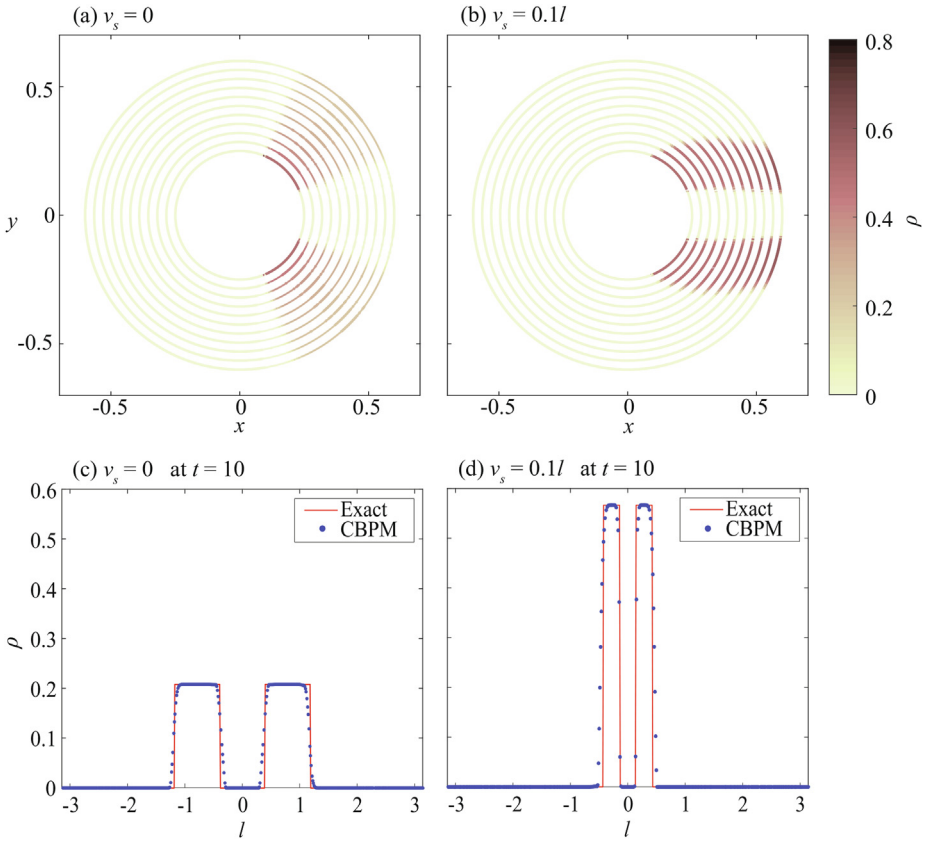

Fig. 4. Expanding circle with $u_n = 0.035$ and with or without tangential velocity: comparison between CBPM simulations and exact solutions. (a) and (b) Solution obtained using CBPM with $v_S = 0$ and $v_S = 0.1l$, respectively, with interface shown at regular time intervals ($\Delta T = 1$). (c) and (d) Exact and CBPM solution density representation over arc length parameter at $t = 10$ with $v_S = 0$ and $v_S = 0.1l$, respectively. The discretisation used is $\Delta x = 0.01$ and $\Delta t = 0.01$.

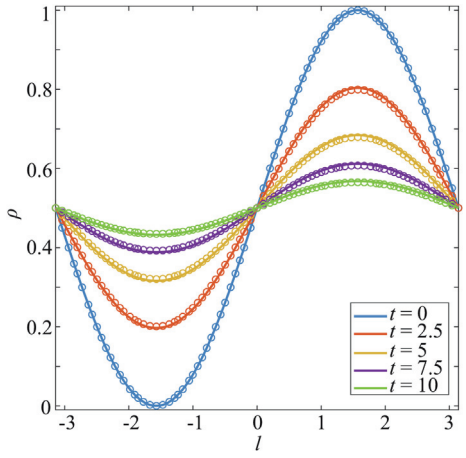

Fig. 5. Analytic (solid line) and CBPM (points) solutions for diffusion around a stationary circle. The discretisation used is $\Delta x = 0.01$ and $\Delta t = 0.01$.

inwards. The results in Fig. 6f illustrate how one may explain a change in anisotropic tissue material properties. As collagen fibrils secreted by osteoblasts may be weaved according to the directionality induced by cell migration, the change in cell trajectory orientation could be used to describe the change in collagen fibre orientation in lamellar bone and the consequent plywood structure (as illustrated in Fig. 1b).

3.3. Bone resorption in basic multicellular units

We now examine the resorption phase of a bone remodelling event as another example where the tangential velocity of cells may be important for the evolution of the tissue interface. In bone resorption, bone tissue is removed by osteoclasts attached to the bone surface. The resorption of bone matrix by osteoclasts creates a cavity which maintains consistent cellular organisation and shape at the resorption front (Fig. 1c) (Jaworski and Hooper, 1980; Ryser et al., 2009; Buenzli et al., 2010; Buenzli et al., 2011; Buenzli et al., 2014; Buenzli et al., 2012; Lassen et al., 2017). We apply our tissue growth model to this situation to show that to maintain this stable travelling resorption front, directed tangential osteoclast motion is required (Fig. 1c).

Recent works have suggested that osteoclasts at the front of basic multicellular units may remain at this position for a long period of time (Lassen et al., 2017), unlike previous suggestions that osteoclasts move down the cavity walls (Burger et al., 2003; Buenzli et al., 2012). We show here, based on simple numerical simulations, that a stable resorption front requires cell guidance mechanisms to steer osteoclasts back toward the tip of the cavity (Fig. 1c). Without such directed motion, the cavity rapidly expands out and osteoclasts move away from each other (Fig. 7a). Figs. 7b and 7c show numerical simulations where two different types of signals are used to steer osteoclasts back toward the tip of the cavity. The first signal modelled can be thought of as haptotaxis, which is a cell guidance mechanism in response to adhesion gradient on the substrate generated by cell binding to substrate molecules

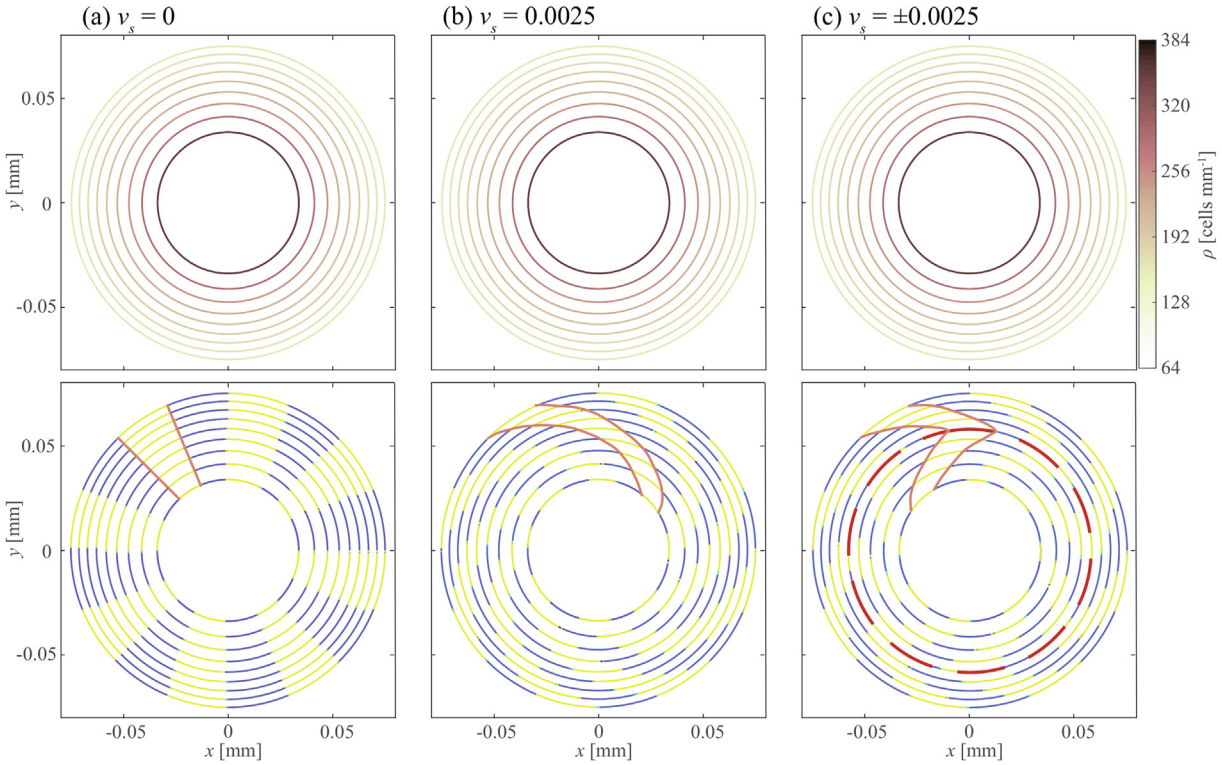

Fig. 6. Circular pore infilling results with cell secretion rate $k = 7.8125\text{e}-06\,\text{mm/day}$ and with varying tangential cell velocity. In each figure the initial interface is the outermost ring and the interface is shown at regular time intervals ($\Delta T = 3\,\text{days}$). The top figures show density and interface position while the bottom figures show cell trajectory tracking and interface position with a single cell trajectory annotated in orange. (a) Infilling circle without tangential velocity. (b) Infilling circle with tangential velocity $v_s = 0.0025\,\text{mm/day}$. (c) Infilling circle with tangential velocity $v_s = 0.0025\,\text{mm/day}$ when $t < 12.5\,\text{days}$ and $v_s = -0.0025\,\text{mm/day}$ when $t \geqslant 12.5\,\text{days}$. The location of the change of direction is emphasised in a red dashed circle. The discretisation used is $\Delta x = 0.001\,\text{mm}, \Delta t = 0.075\,\text{days}$.

(Davies, 2013). The second is chemotaxis, which describes cell guidance through a chemical gradient (Murray, 2002). These signals inducing cell tangential velocity could originate from mechanical signals, believed to be important in guiding bone remodelling processes in bone. Around the tip of the resorption cavity, mechanical stresses are increased (Smit and Burger, 2000; Ruimerman et al., 2005). Osteocytes, which form a network within bone matrix are able to sense mechanical deformation and transduce these mechanical variables into molecular signals. These molecular signals may then diffuse through bone matrix and in the resorption cavity, where they are sensed by the osteoclasts as a chemotactic signal. Alternatively, mechanical gradients along the resorption cavity walls may be felt directly by osteoclasts as a haptotacic signal.

Osteoclasts work in close contact with other cells lining the cavity walls, called reversal cells, which may provide haptotactic signals such as receptor activator of nuclear factor kappa-B ligand (RANKL) (Martin et al., 2004; Lassen et al., 2017). Here we assume the haptotactic signal induces a tangential velocity to the osteoclasts, $v_s = a\,l$, where l is the arc length measured along the cavity wall from the tip and a is a positive constant. This is similar to Section 3.2 where $l > 0$ on the upper part of the cavity and $l < 0$ on the lower part of the cavity. Using this form of tangential cell velocity, it can be seen from Fig. 7b, that a stable resorption front is formed. Between $t = 0$ and approximately $t = 3\,\text{days}$, there is a transient period, where the shape of the resorption front evolves until a balance between the advection-induced crowding and curvature-induced spreading of the osteoclasts is achieved. After this transient, the cell density profile and the cavity front shape is maintained as it progresses through the bone tissue.

Alternatively, we model chemotaxis by projecting a velocity gradient field, such as one created by a gradient of chemical concentration $-b\nabla C$, onto the cavity surface and taking this projection as the tangential velocity,

$$v_S = -b\nabla C \cdot \boldsymbol{\tau}. \tag{20}$$

Indeed, active osteoclasts remain bound to the interface, therefore they can only explore the tangential component of the chemical gradient field. This gradient could be due to signalling molecules derived from mechanically-stimulated osteocytes embedded in bone matrix, that steer osteoclasts toward specific areas of bone needing repair (Turner et al., 1994; Marotti, 2000; Ryser et al., 2009; Lerebous and Buenzli, 2016), such as high mobility group box protein 1 (HMGB1) (Yang et al., 2008) and colony-stimulating factor 1 (CSF-1) (Harris et al., 2012), or it may be due to other chemotactic molecules from the bone microenvironment, such as monocyte chemoattractant protein-1 (MCP-1/CCL2) (Wu et al., 2013), and the chemorepulsing sphingosine-1-phosphate (S1P) (Ishii et al., 2010). For the results presented here, we simply take $-b\nabla C = [0, -2.5\ \text{sgn}(y)y^2]$, which is a velocity field in the y direction with streamlines pointing towards the centerline of the cavity. Fig. 7c shows that, similarly to the haptotaxis results, stable resorption front behaviour is obtained after an adjustment period between $t = 0$ and $t = 3\,\text{days}$.

Both forms of cell guidance signal result in stable resorption fronts, but they lead to different resorption cavity shapes, indicating that the type of signal is also important for the resorption front. The chemotactic signal results in a wider distribution of osteoclasts around the resorption front compared to the haptotactic signal, which results in a high concentration of cells on a narrow portion of the interface. Due to coupling, these differences in cell densities are reflected in the shape of the resorption fronts. However, the speed of these resorption fronts is comparable, with the haptotactic signal canal reaching $x \approx 0.345\,\text{mm}$ at $t = 12\,\text{days}$ and the

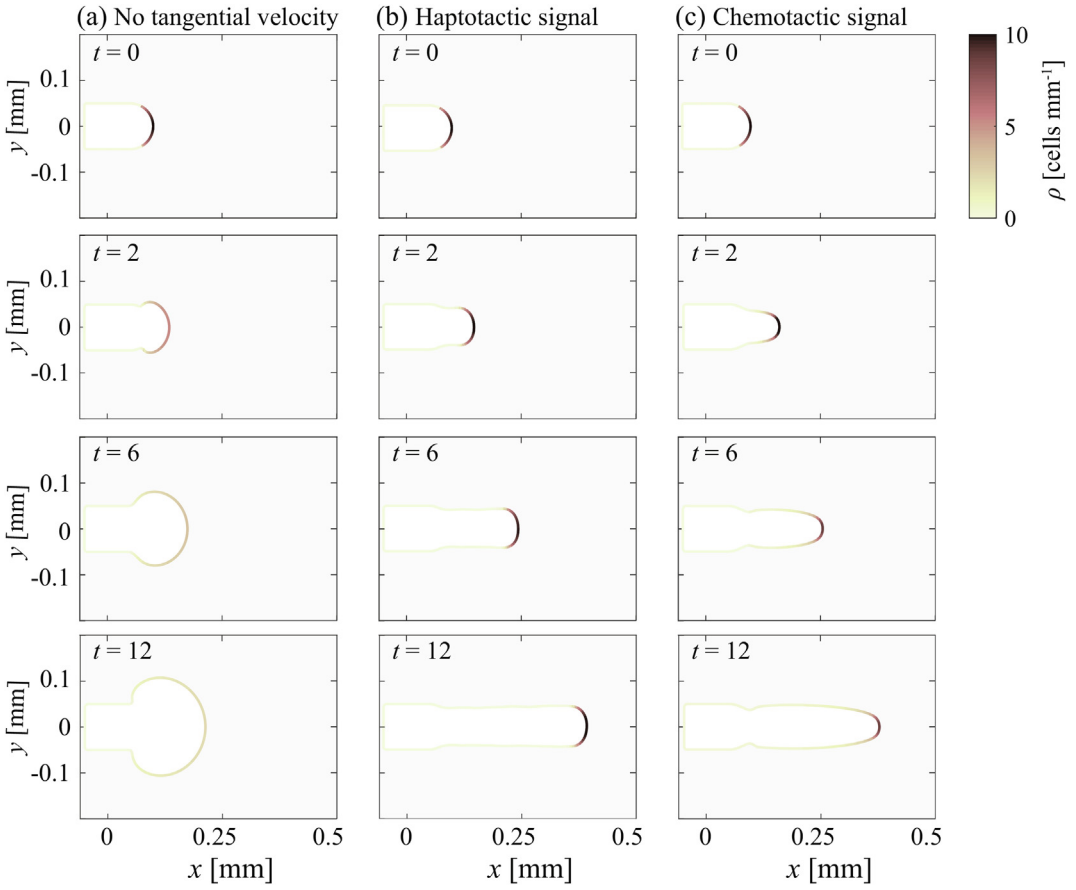

Fig. 7. Bone resorption results with different forms of tangential cell advection. The time is shown in days and the spatial unit is mm. The resorption rate is 0.025 mm/day ($k = -0.025$). (a) Resorption front behaviour with no tangential velocity pulling cells. (b) Haptotactic signal: arc length dependent tangential velocity. The proportionality constant between the arc length distance and the tangential velocity is $a = 0.6$. (c) Chemotactic signal: tangential velocity determined by the projection of an external gradient field on the interface. The discretisation used is $\Delta x = 0.00375, \Delta t = 0.02$.

chemotactic signal canal reaching $x \approx 0.34$ mm at $t = 12$ days. These speeds align well with expected speeds of resorption cavities (30–40 μm/day) (Jaworski et al., 1981; Lassen et al., 2017). A combination of both signals is also possible, and leads to similar conclusions (Supplementary Information, Section S2). The effect of changing parameter values for the haptotactic and chemotactic signals is also shown in the Supplementary Information (Figure S2). The diameter of the simulated resorption cavities falls within the values stated in the analysis of exerimental resorption cavities by Lassen et al. (2017). In our simulations, the 'Level 1' canal diameters (25 μm from the front) are 58.8 μm for the chemotaxis and 87.7 μm for the haptotaxis, and the 'Level 2' canal diameters (325 μm from the front) are around 100 μm for both chemotaxis and haptotaxis. The range of diameters found in Lassen et al. (2017) for Level 1 is 30–180 μm with the mean being 80 μm and for Level 2 it is 110–390 μm with the mean being 200 μm.

3.4. Root hair growth

We now apply our model to the apical growth of root hairs. Root hairs have a single tip-growing cell which concentrates secretory vesicles to the tip of the cell (Miller et al., 1997). To apply our model to this situation, we take the underlying surface to be the root hair cell membrane, and the surface density ρ to represent the density of secretory vesicles near the root hair cell membrane (Shaw et al., 2000). We assume that the cell membrane only has a normal velocity, as described by Eq. 1 and as suggested by experimental observations (Fig. 8c), and that the secretory vesicles have a tangential velocity determined by a haptotatic signal ($v_s = al$). This tangential velocity allows the position of the vesicles to be maintained near the tip of the cell (Shaw et al., 2000). By tracking the material points of the root hair cell membrane in time in our model, we see very similar trajectories to those observed in the growing root hairs analysed in Shaw et al. (2000), where microspheres adhering to the cell membrane were used to track the evolution of its material points (Figs. 8a and c). Without tangential velocity, the secretory vesicles would also follow these trajectories and the cell would not grow its tip only in the longitudinal direction. Furthermore, the curvature of the membrane around the growing tip reflects the curvature map measured in growing root hairs (Shaw et al., 2000), where highest curvature if found a small distance away from the tip centre (Figs. 8b and d). This example application shows that the addition of tangential velocity to the tissue growth model allows for multiple different new applications of tissue growth to be explored.

4. Discussion and conclusion

Tangential cell motion generated by cell guidance mechanisms is important in several situations of tissue growth, such as growth occurring at an angle with respect to the tissue surface, and the generation of anisotropic tissue properties. We have developed a new mathematical model for tissue growth under collective curvature control to incorporate such directed cell guidance mechanisms by including tangential cell motion. The model is derived from conservation principles applied to the surface density of

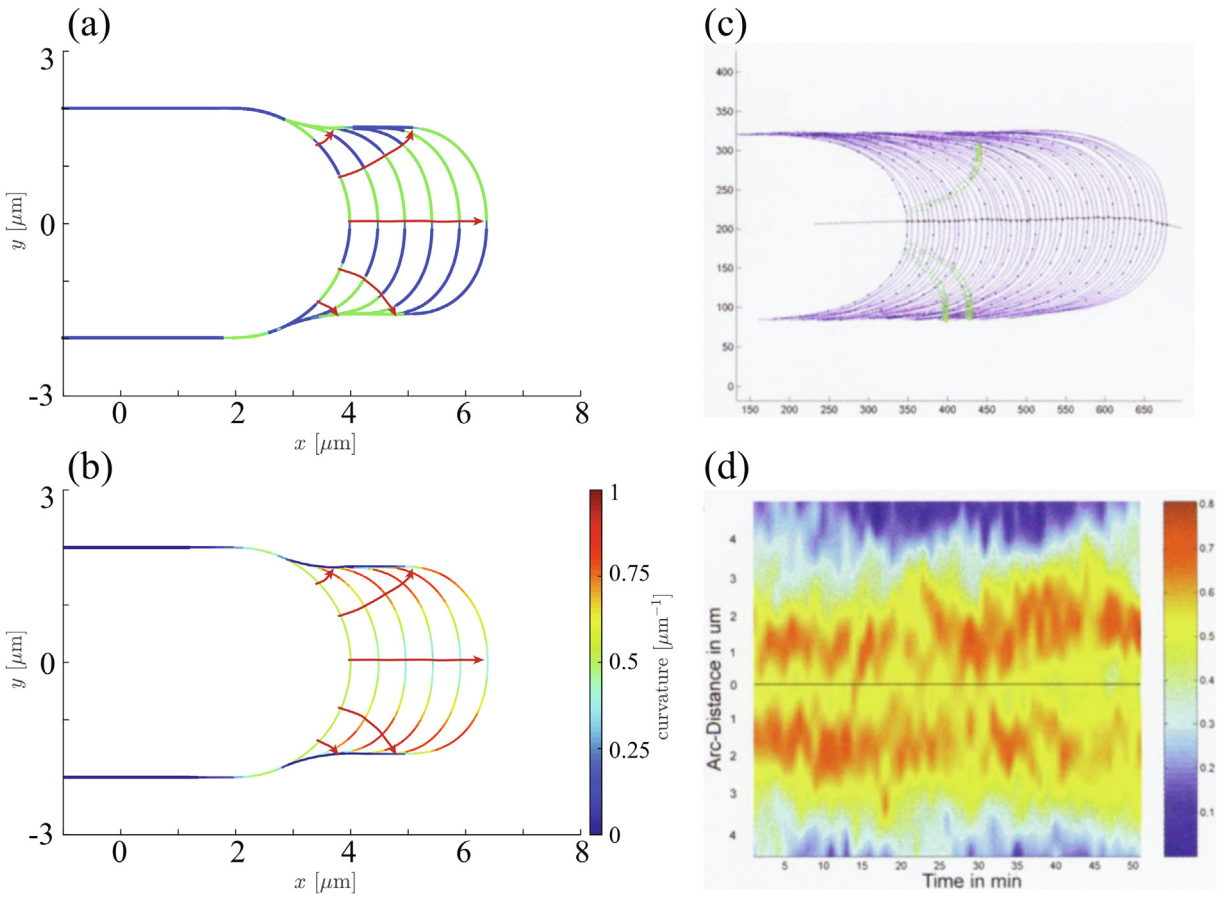

Fig. 8. Apical growth of root hair cells. (a) The numerically simulated root hair cell membrane is shown every 5 min intervals, assuming a secretory rate of 0.1μm/minute. Material points of the cell membrane are stained in blue or green and their trajectories are highlighted in red. (b) Curvature map along the numerically simulated cell membranes. (c) Experimental material point tracking results (green) for a 36 min tracking experiment (reproduced with permissions from Shaw et al. (2000)). (d) Curvature map versus arc distance from the root hair centre over time (reproduced with permissions from Shaw et al. (2000)).

tissue-synthesising cells. This derivation results in a PDE for cell density on a moving boundary, which is coupled with the boundary motion. The governing equations are expressed in covariant form, that is, they are independent of a choice of surface parameterisation and coordinate system. We solve the model numerically using a hybrid front-tracking computational method, the CBPM, and find good agreement with analytic solutions.

Experimentally, the interaction between curvature control of tissue growth and directed cell motion is difficult to investigate, due to the challenge of controlling evolving tissue geometries. Crowding and spreading effects on rates of tissue progression are a consequence of space constraints that may be masked by cell behavioural influences in experiments. The development of mathematical models that account for such collective effects can help disentangle geometric and cell behavioural influences of tissue growth (Cai et al., 2007; Alias, 2018; Buenzli et al., 2020). The example of bone tissue resorption developed in this paper (Fig. 7) illustrates the importance of taking into consideration both the mechanistic influence of curvature on osteoclast density, and the tangential motion of osteoclasts with respect to the bone interface. Without accounting for the mechanistic influence of curvature, the presence of a driving force steering osteoclasts toward the centerline of the resorption cavity would not be highlighted. Without tangential motion of osteoclasts at the tip of bone resorption cavities, our results suggest that stable cavity shapes are not possible.

Our mathematical model describes the joint evolution of the tissue interface and tissue-synthesising cell density. The example of bone pore infilling in Fig. 6 illustrates that directed motion of cells can generate anisotropies in tissue material properties. While we did not model tissue generation explicitly, our model may be coupled with more detailed tissue generation mechanisms that include creation and destruction of tissue material at moving interfaces, as well as tissue maturation mechanisms, based on bulk and surface mass balance (Cumming et al., 2010; Buenzli, 2015; Buenzli, 2016). Our model thus provides a basis for further explorations into the relationship between the spatial organisation of anisotropic tissue material properties, and the dynamics of their creation. Biological experimental data often takes the form of tissue samples or biopsies representing single snapshots in time of the state of the tissue. This type of data contains detailed spatial information about the organisation of a tissue, but it does not offer a detailed picture of its time evolution. The provision of mathematical links between features recorded in the state of a tissue and the dynamics of its formation may allow us to deduce how a tissue has been produced given an analysis of its material properties. In bone tissues, for example, several features of bone formation are recorded, such as osteocyte density (Buenzli, 2015), mineral density (Buenzli, 2016; Lerebours et al., 2020), and tetracycline labels and lamellae, which provide information about past location of the bone interface (Martin et al., 2004; Buenzli et al., 2014; Andreasen C.M. et al., 2018). This type of information is used in bioarcheology to estimate archaeological age and activity (Buckberry and Chamberlain, 2002; Maggiano et al., 2008; Mays, 2010). An analysis of lamellae patterns in bone cross sections could provide more information about osteoblast behaviour, and provide more insights

in cases of irregular bone formation patterns such as drifting osteons (Robling and Stout, 1999; Maggiano, 2012) and bone disorders.

Discretising PDEs on moving boundaries is a challenging problem of applied mathematics. In this paper, we restricted our model to two dimensional applications for simplicity. Clearly, applications of our model to three-dimensional tissue growth are of interest (Fig. 1) (Guyot et al., 2014; Goriely, 2017; Ambrosi et al., 2019; Ehrig et al., 2019). Sophisticated techniques have been developed to simulate the evolution of interfaces in three-dimensional complex systems (Sethian, 1999; Tryggvason et al., 2001; Glimm et al., 1999; Shin and Juric, 2002; Osher and Fedkiw, 2003; Du et al., 2006; Leung and Zhao, 2009; Hon et al., 2014). While the level-let-like method developed in (Alias and Buenzli, 2019) for curvature-controlled tissue growth may be suitably adapted to include tangential cell velocity, the CBPM of Hon et al. (2014) used in this work is also applicable to three-dimensional interfaces.

CRediT authorship contribution statement

Solene G.D. Hegarty-Cremer: Conceptualization, Methodology, Writing - review & editing, Writing - original draft, Software, Validation, Formal analysis, Investigation, Visualization. **Matthew J. Simpson:** Conceptualization, Methodology, Formal analysis, Writing - review & editing, Supervision, Project administration, Funding acquisition. **Thomas L. Andersen:** Resources, Methodology, Formal analysis, Writing - review & editing, Funding acquisition. **Pascal R. Buenzli:** Conceptualization, Methodology, Formal analysis, Writing - review & editing, Supervision, Project administration, Funding acquisition.

Declaration of Competing Interest

The authors declare that they have no known competing financial interests or personal relationships that could have appeared to influence the work reported in this paper.

Acknowledgements

This work is supported by the Australian Research Council (DP180101797, DP200100177), the Centre for Biomedical Technologies, Queensland University of Technology (QUT), and the Institute of Health and Biomedical Innovation (IHBI), QUT, as well as the VELUX foundation (Project No. 25723). We thank the three anonymous referees for their helpful comments.

Appendix A. Evolution of local surface area

We start with the equation for the rate of change of a vector area element ($\delta\mathbf{S} = \mathbf{n}\delta S$) of a material surface from Batchelor (1967),

$$\left(\frac{\partial(\delta\mathbf{S})}{\partial t}\right)_{\mathbf{m}} = (\nabla\cdot\mathbf{u})\delta\mathbf{S} - (\nabla\mathbf{u})^{\mathrm{T}}\delta\mathbf{S}, \tag{A.1}$$

where $\nabla\mathbf{u}$ is the Jacobian matrix of $\mathbf{u}$. Following Stone (1990), we take the inner product with $\mathbf{n}$, to obtain an expression for the change in local surface area, δS, over time,

$$\left(\frac{\partial(\delta S)}{\partial t}\right)_{\mathbf{m}} = \delta S\left[\nabla\cdot\mathbf{u} - \mathbf{n}^{\mathrm{T}}(\nabla\mathbf{u})\ \mathbf{n}\right]. \tag{A.2}$$

The right hand side of Eq. (A.2) corresponds to subtracting to the total divergence of $\mathbf{u}$, that is, to the trace of the Jacobian matrix of $\mathbf{u}$, the normal component of the trace, $\mathbf{n}^{\mathrm{T}}(\nabla\mathbf{u})\ \mathbf{n} = \mathbf{n}^{\mathrm{T}}(\nabla\mathbf{u})^{\mathrm{T}}\ \mathbf{n}$. This gives the surface divergence operator of $\mathbf{u}$, so that

$$\left(\frac{\partial(\delta S)}{\partial t}\right)_{\mathbf{m}} = \delta S\nabla_S\cdot\mathbf{u} \tag{A.3}$$

Decomposing $\mathbf{u}$ into its tangential and normal components, $\mathbf{u} = u_n\mathbf{n} + \mathbf{u}_S$, one gets

$$\left(\frac{\partial(\delta S)}{\partial t}\right)_{\mathbf{m}} = \delta S(\nabla_S\cdot(u_n\mathbf{n}) + \nabla_S\cdot\mathbf{u}_S) = \delta S(u_n\kappa + \nabla_S\cdot\mathbf{u}_S) \tag{A.4}$$

where the second equality in Eq (A.4) uses the fact that the surface divergence of the unit normal vector is the mean curvature of the surface, $\kappa = \nabla_S\cdot\mathbf{n}$ (Goldman, 2005), and that the surface gradient is perpendicular to $\mathbf{n}$, so that $\mathbf{n}\cdot\nabla_S u_n = 0$.

Appendix B. Comparison with the literature

In multiphase physico-chemical systems, similar evolution equations to Eq. (11) are derived for the surface transport of surfactants at the interface between two phases (Stone, 1990; Wong et al., 1996; Xu and Zhao, 2003). A difference between such physical systems and the biological systems we are modelling is the coupling between the surface velocities and the cell density via Eq. (1). Cell density affects interface evolution, whereas in multiphase physico-chemical systems, surface evolution is usually assumed to be independent of surfactant density. Furthermore physico-chemical system models do not consider the tangential velocity of a surfactant with respect to the surface.

In Stone (1990), surfactant mass balance equations are derived, however the nature of the time derivative of surfactant density is unclear (Wong et al., 1996). Time derivatives in Stone (1990) implicitly represent changes following paths normal to the interface. The surfactant mass balance results obtained in Wong et al. (1996) make the nature of the time derivative explicit by being derived using an explicit parameterisation of the interface. The parameterisation is general in the sense that the coordinate system is not necessarily bound to the material points of the interface. If we set $\mathbf{v}_S = 0, A = P = 0$ in Eq. (13), we fall back on Eq. (7) from Stone (1990) following normal trajectories, and Eq. (5b) from Wong et al. (1996) equation if the timelines of their parameterisation are taken to be following the normal trajectories of the surface.

Neither the equations in Wong et al. (1996) nor Stone (1990) include coupling between the interface speed and density of cells nor tangential velocity. The derivation in Alias (2017) includes coupling between cell density and interface speed, but the cells have no tangential advection, that is, their only lateral motion is diffusive. To compare our model with that in Alias (2017), the cell velocities in Eq. (13) must be chosen such that the cells move along the normal trajectories of the interface. Therefore, if we set $v_S = -u_S$, the governing equations agree.

Appendix C. Supplementary data

Supplementary data associated with this article can be found, in the online version, athttps://doi.org/10.1016/j.jtbi.2021.110658.

References

Alias, M.A., Buenzli, P.R., 2017. Modeling the Effect of Curvature on the Collective Behavior of Cells Growing New Tissue. Biophys. J . 112, 193–204. https://doi.org/10.1016/j.bpj.2016.11.3203.

Alias, M.A., Buenzli, P.R., 2018. Osteoblasts infill irregular pores under curvature and porosity controls: a hypothesis-testing analysis of cell behaviours. Biomech. Model. Mechanobiol. 17, 1357–1371. https://doi.org/10.1007/s10237-018-1031-x.

Alias, M.A., Buenzli, P., 2019. A level-set method for the evolution of cells and tissue during curvature-controlled growth. Int. J. Numer. Methods Biomed. Eng. 36, (1). https://doi.org/10.1002/cnm.3279 e3279.

Ambrosi, D., Ben Amar, M., Cyron, C., Desimone, A., Goriely, A., Humphrey, J., Kuhl, E., 2019. Growth and remodelling of living tissues: perspectives, challenges and opportunities. J. R. Soc. Interface 16 (157), 20190233. https://doi.org/10.1098/rsif.2019.0233.

Andreasen, C.M., Delaisse, J.-M., van der Eerden, B.C.J., van Leeuwen, J.P.T.M., Ding, M., Andersen, T.L., 2018. Understanding Age-Induced Cortical Porosity in Women: The Accumulation and Coalescence of Eroded Cavities Upon Existing Intracortical Canals Is the Main Contributor. J. Bone Miner. Res. 33 (4), 606–620. https://doi.org/10.1002/jbmr.3354.

Arnoldus, H., 2006. Conservation of charge at an interface. Opt. Commun. 265 (1), 52–59. https://doi.org/10.1016/j.optcom.2006.03.024.

Batchelor, G.K., 1967. An Introduction to Fluid Dynamics. Cambridge U.P, Cambridge.

Berger, M., 2003. A Panoramic View of Riemannian Geometry. Springer, Berlin. 10.1007/978-3-642-18245-7_10..

Bidan, C., Kommareddy, K., Rumpler, M., Kollmannsberger, P., Bréchet, Y., Fratzl, P., Dunlop, J., Roeder, R., 2012. How Linear Tension Converts to Curvature: Geometric Control of Bone Tissue Growth (Geometric Control of Bone Tissue Growth). PLoS ONE 7, (5). https://doi.org/10.1371/journal.pone.0036336 e36336.

Bidan, C.M., Kommareddy, K.P., Rumpler, M., Kollmannsberger, P., Fratzl, P., Dunlop, J.W., 2015. Geometry as a factor for tissue growth: towards shape optimization of tissue engineering scaffolds. Adv. Healthcare Mater. 2 (1), 186–194. https://doi.org/10.1002/adhm.201200159.

Bidan, C.M., Kollmannsberger, P., Gering, V., Ehrig, S., Joly, P., Petersen, A., Vogel, V., Fratzl, P., Dunlop, J.W., 2016. Gradual conversion of cellular stress patterns into pre-stressed matrix architecture during in vitro tissue growth. J. R. Soci. Interface 13 (118). https://doi.org/10.1098/rsif.2016.0136.

Buckberry, J., Chamberlain, A., 2002. Age estimation from the auricular surface of the ilium: a revised method. Am. J. Phys. Anthropol. 119 (3), 231–239. https://doi.org/10.1002/ajpa.10130.

Buenzli, P., Pivonka, P., Gardiner, B., Smith, D., Dunstan, C., Mundy, G., 2010. Theoretical analysis of the spatio-temporal structure of bone multicellular units. IOP Conf. Ser.: Mater. Sci. Eng. 10 (1), 10. https://doi.org/10.1088/1757-899X/10/1/012132.

Buenzli, P., Pivonka, P., Smith, D., 2011. Spatio-temporal structure of cell distribution in cortical Bone Multicellular Units: A mathematical model. Bone 48 (4), 918–926. https://doi.org/10.1016/j.bone.2010.12.009.

Buenzli, P., Pivonka, P., Smith, D., 2014. Bone refilling in cortical basic multicellular units: Insights into tetracycline double labelling from a computational model. Biomech. Model. Mechanobiol. 13 (1), 185–203. https://doi.org/10.1007/s10237-013-0495-y.

Buenzli, P., 2015. Osteocytes as a record of bone formation dynamics: A mathematical model of osteocyte generation in bone matrix. J. Theor. Biol. 364, 418–427. https://doi.org/10.1016/j.jtbi.2014.09.028.

Buenzli, P., 2016. Governing Equations of Tissue Modelling and Remodelling: A Unified Generalised Description of Surface and Bulk Balance. PLoS One 11, (4). https://doi.org/10.1371/journal.pone.0152582 e0152582.

Buenzli, P., Jeon, J., Pivonka, P., Smith, D., Cummings, P., 2012. Investigation of bone resorption within a cortical basic multicellular unit using a lattice-based computational model. Bone 50 (1), 378–389. https://doi.org/10.1016/j.bone.2011.10.021.

Buenzli, P., Lanaro, M., Wong, C., Mclaughlin, M., Allenby, M., Woodruff, M., and Simpson, M., 2020. Cell proliferation and migration explain pore bridging dynamics in 3D printed scaffolds of different pore size. In Press, Acta Biomaterialia. BioRxiv. https://doi.org/10.1101/2020.03.12.989053.

Burger, E., Klein-Nulend, J., Smit, T., 2003. Strain-derived canalicular fluid flow regulates osteoclast activity in a remodelling osteon—a proposal. J. Biomech. 36 (10), 1453–1459. https://doi.org/10.1016/S0021-9290(03)00126-X.

Cai, A.Q., Landman, K.A., Hughes, B.D., 2007. Multi-scale modeling of a wound-healing cell migration assay. J. Theor. Biol. 245, 576–594.

Callens, S.J.P., Uyttendaele, R.J.C., Fratila-Apachitei, L.E., Zadpoor, A.A., 2020. Substrate curvature as a cue to guide spatiotemporal cell and tissue organization. Biomaterials 232, 1–22. https://doi.org/10.1016/j.biomaterials.2019.119739.

Chaudhuri, O., Gu, L., Klumpers, D., Darnell, M., Bencherif, S.A., Weaver, J.C., Huebsch, N., Lee, H.-P., Lippens, E., Duda, G.N., 2016. Hydrogels with tunable stress relaxation regulate stem cell fate and activity. Nat. Mater. 15 (3), 326–334. https://doi.org/10.1038/nmat4489.

Cumming, B.D., McElwain, D.L.S., Upton, Z., 2010. A mathematical model of wound healing and subsequent scarring. J. R. Soc. Interface 7, 19–34.

Curtis, A.S., Varde, M., 1964. Control of cell behavior: topological factors. J. Natl Cancer Inst. 33 (1), 15–26. https://doi.org/10.1093/jnci/33.1.15.

Davies, J., 2013. Mechanisms of morphogenesis. Academic Press, Amsterdam.

Deligianni, D.D., Katsala, N.D., Missirlis, Y.F., 2001. Effect of surface roughness of hydroxyapatite on human bone marrow cell adhesion, proliferation, differentiation and detachment strength. Biomaterials 22, 87–96. https://doi.org/10.1016/S0142-9612(00)00174-5.

Discher, D.E., Janmey, P., Wang, Y.-L., 2005. Tissue cells feel and respond to the stiffness of their substrate. Science 310 (5751), 1139–1143. https://doi.org/10.1126/science.1116995.

Du, J., Fix, B., Glimm, J., Jia, X., Li, X., Li, Y., Wu, L., 2006. A simple package for front tracking. J. Comput. Phys. 213, 613–628.

Dzobo, K., Thomford, N.E., Senthebane, D.A., Shipanga, H., Rowe, A., Dandara, C., Pillay, M., Motaung, K.S., 2018. Advances in Regenerative Medicine and Tissue Engineering: Innovation and Transformation of Medicine. Stem Cells Int. 2018,. https://doi.org/10.1155/2018/2495848 2495848.

Ehrig, S., Schamberger, B., Bidan, C., West, A., Jacobi, C., Lam, K., Kollmannsberger, P., Petersen, A., Tomancak, P., Kommareddy, K., Fischer, F.D., Fratzl, P., Dunlop, J., 2019. Surface tension determines tissue shape and growth kinetics. Sci. Adv. 5 (9). https://doi.org/10.1126/sciadv.aav9394. eaav9394.

Engler, A.J., Sen, S., Sweeney, H.L., Discher, D.E., 2006. Matrix elasticity directs stem cell lineage specification. Cell 126 (4), 677–689. https://doi.org/10.1016/j.cell.2006.06.044.

Evans, L., 2010. Partial differential Eqs. American Mathematical Society, Providence, R.I.

Dunn, G.A., Heath, J.P., 1976. A new hypothesis of contact guidance in tissue cells. Exp. Cell Res. 101 (1), 1–14. https://doi.org/10.1016/0014-4827(76)90405-5.

Gamsjäger, E., Bidan, C., Fischer, F., Fratzl, P., Dunlop, J., 2013. Modelling the role of surface stress on the kinetics of tissue growth in confined geometries. Acta Biomater. 9 (3), 5531–5543. https://doi.org/10.1016/j.actbio.2012.10.020.

Glimm, J., Li, X.L., Liu, Y., Zhao, N., 1999. Conservative front tracking and level set algorithms. Proc. Nat. Acad. Sci. 98, 14198–14201.

Goldman, R., 2005. Curvature formulas for implicit curves and surfaces. Computer Aided Geometric Design 22 (7), 632–658. https://doi.org/10.1016/j.cagd.2005.06.005.

Goriely, A., 2017. The Mathematics and Mechanics of Biological Growth. Springer Science+Business Media, New York.

Guyot, Y., Papantoniou, I., Chai, Y.C., Van Bael, S., Schrooten, J., Geris, L., 2014. A computational model for cell/ECM growth on 3D surfaces using the level set method: a bone tissue engineering case study. Biomech. Model. Mechanobiol. 13 (6), 1361–1371. https://doi.org/10.1007/s10237-014-0577-5.

Haeger, A., Wolf, K., Zegers, M., Friedl, P., 2015. Collective cell migration: guidance principles and hierarchies. Trends Cell Biol. 25 (9), 556–566. https://doi.org/10.1016/j.tcb.2015.06.003.

Harris, S.E., MacDougall, M., Horn, D., Woodruff, K., Zimmer, S.N., Rebel, V.I., Fajardo, R., Feng, J.Q., Gluhak-Heinrich, J., Harris, M.A., Abboud Werner, S., 2012. Meox2Cre-mediated disruption of CSF-1 leads to osteopetrosis and osteocyte defects. Bone 50 (1), 42–53. https://doi.org/10.1016/j.bone.2011.09.038.

Hegarty-Cremer S.G.D., 2020. CBPM_curvature_and_cell_guidance, GitHub repository. https://github.com/SoleneHC/CBPM_curvature_and_cell_guidance.

Hon, S., Leung, S., Zhao, H., 2014. A cell based particle method for modeling dynamic interfaces. J. Comput. Phys. 272, 279–306. https://doi.org/10.1016/j.jcp.2014.04.032.

Ishii, M., Kikuta, J., Shimazu, Y., Meier-Schellersheim, M., Germain, R.N., 2010. Chemorepulsion by blood S1P regulates osteoclast precursor mobilization and bone remodeling in vivo. J. Exp. Med. 207 (13), 2793–2798. https://doi.org/10.1084/jem.20101474.

Jaworski, Z.F.G., Hooper, C., 1980. Study of cell kinetics within evolving secondary Haversian systems. J. Anat. 131 (1), 91–102.

Jaworski, Z.F.G., Duck, B., Sekaly, G., 1981. Kinetics of osteoclasts and their nuclei in evolving secondary Haversian systems. J. Anat. 133 (3), 397–405.

Kollmannsberger, P., Bidan, C.M., Dunlop, J.W.C., Fratzl, P., 2011. The physics of tissue patterning and extracellular matrix organisation: how cells join forces. Soft Matter 7 (20), 9549–9560. https://doi.org/10.1039/c1sm05588g.

Lassen, N., Andersen, T., Ploen, G., Soe, K., Hauge, E., Harving, S., Eschen, G.E.T., Delaisse, J., 2017. Coupling of Bone Resorption and Formation in Real Time: New Knowledge Gained From Human Haversian BMUs. J. Bone Miner. Res. 32 (7), 1395–1405. https://doi.org/10.1002/jbmr.309.

Lerebous, C., Buenzli, P.R., 2016. Towards a cell-based mechanostat theory of bone: the need to account for osteocyte desensitisation and osteocyte replacement. J. Biomech. 49, 2600–2606.

Lerebours, C., Weinkamer, R., Roschger, A., Buenzli, P.R., 2020. Mineral density differences between femoral cortical bone and trabecular bone are not explained by turnover rate alone. Bone Reports 13,. https://doi.org/10.1101/2020.06.08.141036 100731.

Leung, S., Zhao, H., 2009. A grid based particle method for moving interface problems. J. Comput. Phys. 228 (8), 2993–3024. https://doi.org/10.1016/j.jcp.2009.01.005.

Leung, S., Lowengrub, J., Zhao, H., 2011. A grid based particle method for solving partial differential equations on evolving surfaces and modeling high order geometrical motion. J. Comput. Phys. 230 (7), 2540–2561. https://doi.org/10.1016/j.jcp.2010.12.029.

Livne, A., Bouchbinder, E., Geiger, B., 2014. Cell reorientation under cyclic stretching. Nature Commun. 5 (1), 3938. https://doi.org/10.1038/ncomms4938.

Lo, C.M., Wang, H.B., Wang, Y.L., 2000. Cell movement is guided by the rigidity of the substrate. Biophys. J . 79 (1), 144–152. https://doi.org/10.1016/S0006-3495(00)76279-5.

Lowengrub, J.S., Frieboes, H.B., Cristini, V., 2010. Nonlinear modelling of cancer: bridging the gap between cells and tumours. Nonlinearity 23 (1), R1–R91. https://doi.org/10.1088/0951-7715/23/1/R01.

Maggiano, I.S., Schultz, M., Kierdorf, H., Sosa, T.S., Maggiano, C.M., Tiesler Blos, V., 2008. Cross-sectional analysis of long bones, occupational activities and long-distance trade of the classic maya from Xcambó—Archaeological and osteological evidence. Am. J. Phys. Anthropol. 136 (4), 470–477. https://doi.org/10.1002/ajpa.20830.

Maggiano, C., 2012. Histomorphometry of Humeral Primary Bone: Evaluating the Endosteal Lamellar Pocket as an Indicator of Modeling Drift in Archaeological and Modern Skeletal Samples. The Ohio State University/OhioLINK.

Marotti, G., 2000. The osteocyte as a wiring transmission system. J. Musculoskelet. Neuronal Interact. 1 (2), 133–136.

Martin, J.Y., Schwartz, Z., Boyan, B.D., 1995. Effect of titanium surface roughness on proliferation, differentiation, and protein synthesis of human osteoblast-like cells (MG63). J. Biomed. Mater. Res. 29 (3), 389–401. https://doi.org/10.1002/jbm.820290314.

Martin, R.B., 2000. Does osteocyte formation cause the nonlinear refilling of osteons? Bone 26, 71–78. https://doi.org/10.1016/S8756-3282(99)00242-2.

Martin, R., Burr, D., Sharkey, N., 2004. Skeletal Tissue Mechanics. Springer Science +Business Media, New York, pp. 32–36.

Mays, S., 2010. The archaeology of human bones. Taylor & Francis; https://books.google.com.my/books?id=s71ocyS3xmUC..

Miller, D., de Ruijter, N.C.A., Emons, A.M.C., 1997. From signal to form: aspects of cytoskeleton-plasma membrane-cell wall continuum in root hair tips. J. Exp. Bot. 48, 1881–1896.

Murray, J., 2002. Mathematical Biology I. An Introduction (Third Edition.). Springer, New York. https://doi.org/10.1007/b98868.

Nelson, C.M., Jean, R.P., Tan, J.L., Liu, W.F., Sniadecki, N.J., Spector, A.A., Chen, C.S., 2005. Emergent patterns of growth controlled by multicellular form and mechanics. Proc. Nat. Acad. Sci. USA 102 (33), 11594–11599. https://doi.org/10.1073/pnas.0502575102.

O'Brien, F., 2011. Biomaterials and scaffolds for tissue engineering. Mater. Today 14 (3), 88–95. https://doi.org/10.1016/S1369-7021(11)70058-X.

Osher, S., Fedkiw, R., 2003. Level set methods and dynamic implicit surfaces. Springer.

Pazzaglia, U., Congiu, T., Marchese, M., Spagnuolo, F., Quacci, D., 2012. Morphometry and Patterns of Lamellar Bone in Human Haversian Systems. Anatomical Record: Adv. Integrative Anatomy Evol. Biol. 295 (9), 1421–1429. https://doi.org/10.1002/ar.22535.

Pelham R.J. Jr., Wang Y.L., 1997. Cell locomotion and focal adhesions are regulated by substrate flexibility.Proceedings of the National Academy of Sciences of the United States of America, 94(25), 13661–13665. https://doi.org/10.1073/pnas.94.25.13661.

Poujade, M., Grasland-Mongrain, E., Silberzan, P., 2007. Collective migration of an epithelial monolayer in response to a model wound. Proc. Nat. Acad. Sci. 104 (41), 15988–15993. https://doi.org/10.1073/pnas.0705062104.

Pressley, A., 2010. Elementary Differential Geometry. Springer, London. https://doi.org/10.1007/978-1-84882-891-9.

Redžić, D.V., 2001. The operator ∇ in orthogonal curvilinear coordinates. Eur. J. Phys. 22 (6), 595–599. https://doi.org/10.1088/0143-0807/22/6/304.

Ripamonti, U., Roden, L., 2010. Biomimetics for the induction of bone formation. Expert Rev. Med. Devices 7 (4), 469–479. https://doi.org/10.1586/erd.10.17.

Robling, A., Stout, S., 1999. Morphology of the Drifting Osteon. Cells Tissues Organs 164 (4), 192–204. https://doi.org/10.1159/000016659.

Rolli, C.G., Nakayama, H., Nakanishi, J., 2012. Switchable adhesive substrates: revealing geometry dependence in collective cell behavior. Biomaterials 33 (8), 2409–2418. https://doi.org/10.1016/j.biomaterials.2011.12.012.

Ruimerman, R., van Rietbergen, B., Hilbers, P.A.J., Huiskes, R., 2005. The effects of trabecular-bone loading variables on the surface signaling potential for bone remodeling and adaptation. Ann. Biomed. Eng. 33 (1), 71–78. https://doi.org/10.1007/s10439-005-8964-9.

Rumpler, M., Woesz, A., Dunlop, J.W., van Dongen, J.T., Fratzl, P., 2008. The effect of geometry on three-dimensional tissue growth. J. R. Soc. Interface 5 (27), 1173–1180. https://doi.org/10.1098/rsif.2008.0064.

Ryser, M., Nigam, N., Komarova, S., 2009. Mathematical Modeling of Spatio-Temporal Dynamics of a Single Bone Multicellular Unit. J. Bone Mineral Res. 24 (5), 860–870. https://doi.org/10.1359/JBMR.081229.

Schrof, S., Varga, P., Galvis, L., Raum, K., Masic, A., 2014. 3D Raman mapping of the collagen fibril orientation in human osteonal lamellae. J. Struct. Biol. 187 (3), 266–275. https://doi.org/10.1016/j.jsb.2014.07.001.

Sethian, J., 1999. Level set methods and fast marching methods: evolving interfaces in computational geometry, fluid mechanics, computer vision, and materials science (2nd ed.). Cambridge, U.K. Cambridge University Press..

Shaw, D., Dumais, J., Long, S., 2000. Cell Surface Expansion in Polarly Growing Root Hairs of Medicago truncatula. Plant Physiol. (Bethesda) 124 (3), 959–969.

Shin, S., Juric, D., 2002. Modeling three-dimensional multiphase flow using a level contour reconstruction method for front tracking without connectivity. J. Comput. Phys. 180, 427–470.

Skalak, R., Dasgupta, G., Moss, M., Otten, E., Dullemeijer, P., Vilmann, H., 1982. Analytical description of growth. J. Theor. Biol. 94 (3), 555–577. https://doi.org/10.1016/0022-5193(82)90301-0.

Skalak, R., Farrow, D., Hoger, A., 1997. Kinematics of surface growth. J. Math. Biol. 35 (8), 869–907. https://doi.org/10.1007/s002850050081.

Smit, B., Burger, E.H., 2000. Is BMU-Coupling a Strain-Regulated Phenomenon? A Finite Element Analysis. J. Bone Miner. Res. 15 (2), 301–307. https://doi.org/10.1359/jbmr.2000.15.2.301.

Stone, H., 1990. A simple derivation of the time-dependent convective-diffusion equation for surfactant transport along a deforming interface. Phys. Fluids A 2 (1), 111–112. https://doi.org/10.1063/1.857686.

Trepat, X., Deng, L., An, S.S., Navajas, D., Tschumperlin, D.J., Gerthoffer, W.T., Butler, J.P., Fredberg, J.J., 2007. Universal physical responses to stretch in the living cell. Nature 447 (7144), 592–595. https://doi.org/10.1038/nature05824.

Wong, H., Rumschitzki, D., Maldarelli, C., 1996. On the surfactant mass balance at a deforming fluid interface. Phys. Fluids 8 (11), 3203–3204. https://doi.org/10.1063/1.869098.

Xu, J., Zhao, H., 2003. An Eulerian Formulation for Solving Partial Differential Equations Along a Moving Interface. J. Sci. Comput. 19 (1), 573–594. https://doi.org/10.1023/A:1025336916176.

Tryggvason, G., Bunner, B., Esmaeeli, A., Juric, D., Al-Rawahi, N., Tauber, W., Hans, J., Nas, S., Jan, Y.-J., 2001. A front-tracking method for the computations of multiphase flow. J. Comput. Phys. 169, 708–759.

Turner, C.H., Forwood, M.R., Otter, M.W., 1994. Mechanotransduction in bone: do bone cells act as sensors of fluid flow?. FASEB J. 8, 875–878.

Wu, A.C., Morrison, N.A., Kelly, W.L., Forwood, M.R., 2013. MCP-1 expression is specifically regulated during activation of skeletal repair and remodeling. Calcif. Tissue Int. 92 (6), 566–575.

Yang, J., Shah, R. Robling, A.G., Templeton, E. Yang, H., Tracey, K.J., Bidwell, J.P., 2008. HMGB1 is a bone-active cytokine. Journal of Cellular Physiology 214(3)730–739; doi: 10.1002/jcp.21268..